Communications in Computational Chemistry
*Commun. Comput. Chem., Vol. 1, No. 2,* 134–144
doi: 10.4208/cicc.2025.90.01


# Two-Dimensional Convolutional Neural Networks for Predicting Non-Markovian Quantum Dissipative Dynamics

Zhiqian Huang[1], Cun Long[2], Qingdong Zhu[1], Jiaan Cao[2] and Xiao Zheng[1,3,*]

[1]*Department of Chemistry, Fudan University, Shanghai 200438, China;*

[2]*Hefei National Research Center for Physical Sciences at the Microscale, University of Science and Technology of China, Hefei, Anhui 230026, China;*

[3]*Hefei National Laboratory, Hefei, Anhui 230088, China.*

[*] Corresponding author: xzheng@fudan.edu.cn

Received on 31 March 2025; Accepted on 15 May 2025

**Abstract:** Simulating non-Markovian quantum dissipative dynamics remains a major challenge in theoretical and computational chemistry. While traditional numerical methods such as hierarchical equations of motion are numerically exact, they suffer from prohibitive computational costs when modeling systems with complex environmental couplings or strong non-Markovian effects. To address this limitation, we propose a deep learning framework based on two-dimensional convolutional neural networks (2D-CNN) for efficiently predicting long-time quantum dissipative dynamics using only short-time trajectory data. Our approach incorporates a 1D-to-2D feature reconstruction strategy, which transforms 1D time-series data into 2D images, and a multi-timescale fusion network to resolve complex dynamical features. We validate the framework on two paradigmatic cases -- dissipative relaxation in a two-level system and Rabi oscillations in a dissipative spin system -- achieving prediction mean absolute errors of $10^{-3}$ and $10^{-2}$, respectively. The results highlight the effectiveness of our 2D-CNN approach in capturing long-time temporal correlations, providing a computationally efficient pathway for simulating quantum dynamics in realistic open systems.

**Key words:** deep learning, quantum dissipative dynamics, convolutional neural network.

## 1. Introduction

Non-Markovian quantum dissipative dynamics is widely observed in various fields ranging from photosynthesis to quantum computing [1-3]. Understanding these dynamics is essential to understand fundamental processes like quantum dissipation, decoherence and energy transfer [4-7]. Despite their universal significance, simulation of long-time open quantum dynamics remains an outstanding challenge, primarily due to the complex non-Markovian memory effects arising from strong system-environment correlations. This persistent theoretical bottleneck highlights the urgent need for developing accurate and computationally feasible methodologies that can simultaneously capture intricate memory effects while maintaining numerical tractability for practical applications.

Over decades, significant progress has been made in developing theoretical methods for modeling non-Markovian quantum dissipative dynamics. Established approaches include: numerical renormalization group (NRG) method [8-12] and its time-dependent extension [13-17], quantum Monte Carlo (QMC) method [18-30], real-time path integral (PI) method [31-37], hierarchical equations of motion (HEOM) [38-46], multi-configuration time-dependent Hartree (MCTDH) [47, 48] and its multilayer extension (ML-MCTDH) [49-53] and second-quantized version [54], density matrix renormalization group (DMRG) method [55-60] and its time-dependent extension [55, 61-65], stochastic quantum dissipation theory methods [66-71], and steady-state density functional theory (i-DFT) method [72]. While these methods have advanced our understanding of open quantum systems, their computational

demands typically scale exponentially with both system size and complexity of environment. This inherent complexity barrier fundamentally restricts applications to large-scale, long-time quantum dynamics. To overcome these limitations, recent efforts have turned to data-driven methods to enhance the efficiency for simulating long-time quantum dissipative dynamics. For instance, the transfer tensor method (TTM) [73-75], pioneered by Cerillo and Cao in 2014, offers a dimensionality-reduction framework to capture the critical dynamics feature by encoding short-time historical evolution into non-Markovian transfer tensors, which can be used to propagate long-time dynamics. Building on this paradigm, machine learning techniques have emerged as promising alternatives for tackling similar challenges.

Machine learning approaches for propagating long-time quantum dynamics can be conceptualized as time series prediction tasks [76], analogous to applications in weather forecasting or financial market modeling. However, quantum dissipative dynamics exhibits a critical distinction: its reduced system dynamics are governed by formally closed quantum dynamical equations rather than intricate real-world processes subjected to noise from countless external sources. The practical tractability stems from the fact that quantum memory effects arise from well-defined environmental interactions. For instance, within the HEOM framework, non-Markovian memory is fully encoded in the environmental hybridization correlation functions.

Recent advances in deep learning have driven a paradigm shift in simulating quantum dissipative dynamics [77-82]. Neural network approaches for time series prediction, including feed-forward neural network (FFNN) [83, 84], recurrent neural networks (RNNs) such as gated recurrent units (GRUs) [85] and long short-term memory networks (LSTMs) [86-88], convolutional neural networks (CNNs) [89-91], and hybrid CNN-LSTM (CNN-LSTM) [92], have demonstrated success in systems like spin-boson models [4, 93] and Fenna-Matthews-Olson (FMO) complexes [94-97]. For example, Lin et al. have applied LSTM to simulate excited-state energy-transfer dynamics, successfully predicting long-time behavior under strong coupling and non-Markovian conditions. By integrating bootstrap sampling with LSTM, they developed a statistical framework to quantify prediction uncertainty and assess model reliability in long-time quantum dynamics simulations [86]. Ullah and Dral have proposed the artificial intelligence quantum dynamics method [90], which uses machine learning to directly predict quantum dynamics trajectories, avoiding the high computational costs and error accumulation inherent to traditional recursive methods. When validated on the FMO complex, the model captured long-time memory effects in quantum dynamics. They further developed a one-shot trajectory learning method [91] based on one-dimensional (1D) CNN, enabling single-step prediction of full trajectories while significantly reducing training time and memory usage. Wu et al. have proposed a 1D-CNN-LSTM based model with feature fusion network for predicting the long-time nonadiabatic quantum dynamics of spin-boson model, achieving high accuracy, robustness and transferability [92]. Furthermore, Zeng et al. have revealed the impact of memory time on the performance of TTM and deep learning approaches and proposed a practical method to estimate the effective memory time [98]. However, determining the appropriate length of short-time historical dynamics in machine learning remains an empirical process. The fundamental principle is to strike a balance between accuracy and efficiency: sufficiently long to encompass key characteristics while as short as possible to minimize resource consumption for training.

By circumventing explicit treatment of system-environment interactions, these methods substantially reduce computational cost while demonstrating unique advantages in long-time dynamics prediction. However, existing methods face certain limitations. For example, their effectiveness in complex systems remains unverified [89-92], such as the Rabi oscillation of a local spin subject to Kondo exchange couplings with environmental spins -- a scenario experimentally demonstrated by Yang et al. [99] and Willke et al. [100] using scanning tunneling microscope-radio frequency (STM-RF) protocols [100-102] to control coherent spin manipulation in hydrogenated Ti atoms and iron phthalocyanine molecules on surfaces. These Rabi oscillations exhibit multi-timescale characteristics, featuring low-frequency oscillations superimposed with high-frequency Larmor precession, and coherence times extending to several hundred nanoseconds (ns). For such complex, long-time quantum dissipative dynamics, RNN architectures risk substantial increases in training costs and complexity due to their inherently sequential nature, which precludes parallelization [103,104]. While 1D-CNNs avoid this issue [105], their long-time prediction accuracy diminishes significantly due to architectural constraints, as discussed in later sections.

To address this challenge, we propose a deep learning framework based on two-dimensional (2D) CNN for accurate long-time dynamics prediction in dissipative quantum systems, including the relaxation of a two-level system and the Rabi oscillations of a local spin. Our approach integrates a "1D-to-2D" temporal reconstruction strategy [106] coupled with multi-timescale feature fusion techniques [92], enhancing the model's ability to capture complex quantum dissipative dynamics.

The remainder of this paper is organized as follows: Section 2 outlines the framework of the 2D-CNN model. Section 3 presents the results and discussion. Section 4 provides the conclusion.

## 2. Theoretical method

Our deep learning model focuses on long-time quantum dissipative dynamics exhibiting multi-timescale characteristics. The architecture of the proposed model is illustrated in **Figure 1**. The inputs consist of a series of reduced density matrix (RDM) elements of the system at discrete times (e.g., $t_1, t_2, t_3, \ldots, t_n$). First, the input undergoes preprocessing to construct datasets compatible with a 2D-

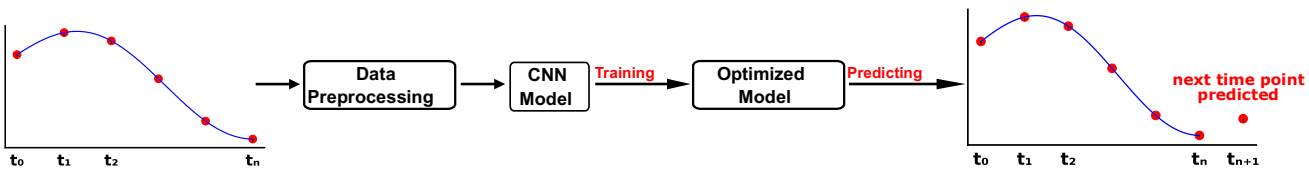


**Figure 1.** Schematic of the quantum dissipative dynamics prediction framework. Reduced density matrix elements at discrete times $(t_1, t_2, t_3, \ldots, t_n)$ are input, preprocessed, and used to train the 2D-CNN model. The optimized model predicts the next discrete time point $t_{n+1}$.

CNN model. These datasets are then fed into the 2D-CNN model for training, resulting in an optimized model that is subsequently used to predict the next time point $t_{n+1}$. Implementation details are described below.

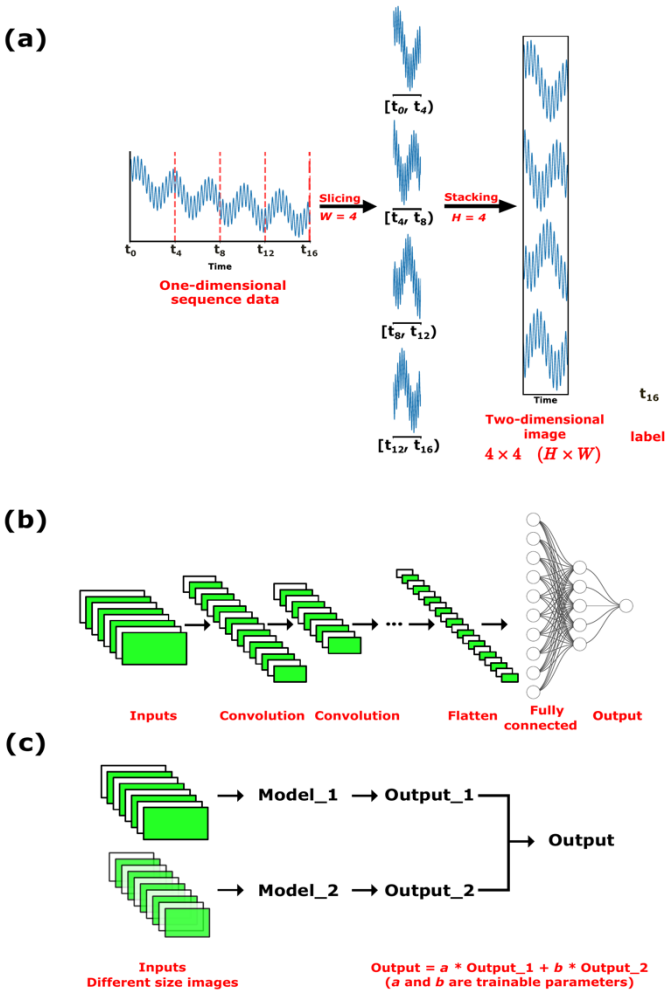


**Figure 2.** Schematic overview of the three core components in our proposed deep learning workflow. (a) Data preprocessing: The original 1D sequential data is first sliced into fixed-length $W$ segments, then vertically stacked with $H$ consecutive segments to form a 2D $H \times W$ image representation. (b) 2D-CNN model: The 2D image is processed through two convolutional layers for feature extraction, followed by flattening and transformation via fully-connected layers to generate preliminary predictions. (c) Multi-timescale feature fusion network: Multi-scale inputs are independently processed through parallel networks, with their outputs aggregated through weighted averaging. The fusion weights are automatically learned during model training.

**Data preprocessing**. As the raw 1D time series data cannot explicitly present two distinct types of variations simultaneously [106], inspired by Wu et al. in Ref. [106], we transform it into 2D images to tackle this limitation. The raw 1D time series data is first partitioned into training and validation sets at a 9:1 ratio. To construct 2D image features, we introduce a sliding-window-based sequence reconstruction method, as illustrated in **Figure 2a**. Specifically, the 1D training sequences are segmented into equal-length fragments using a fixed size of sliding window, which are subsequently stacked vertically along the temporal axis. For example, given the size of sliding window $W = 4$ and the stacking height $H = 4$, the resulting image dimensions become $4 \times 4$ ($H \times W$). The spatial dimensions of input features can be flexibly controlled by adjusting $H$ and $W$. Notably, the preprocessing reverts to raw 1D data when $H = 1$. Each 2D image is labeled with the next time point data from the original sequence. This 1D-to-2D transformation enables the model to effectively capture quantum dissipative dynamics across distinct timescales.

**2D-CNN model**. The structure of our proposed 2D-CNN model is presented in **Figure 2b**, consisting of:

(1) Convolutional layers: Similar to other CNN-based models [89-92], our model also applies two convolutional layers. The first convolutional layer utilizes large-sized kernels with stride matching the kernel dimensions to extract long-time temporal correlations and local spatial patterns. The second convolutional layer employs $1 \times 1$ kernels for feature dimensionality reduction and nonlinear channel-wise interactions while suppressing overfitting through output channel reduction [107].

(2) Flatten layer: To bridge convolutional layers with fully connected layers, a flatten layer is employed to transform 2D feature maps into 1D vectors. While pooling layer that may cause information loss, the flatten layer can preserve the integrity of the original feature dimensions.

(3) Fully connected Layers: Two fully connected layers are implemented. The first integrates high-order features via ReLU activation, and the final layer outputs single-step predictions. Dropout regularization is applied between layers to mitigate overfitting [108, 109].

(4) Multi-timescale feature fusion network: For complex dynamics, the given short-time historical data is often not sufficient to encompass all the necessary information for dynamic evolution, which may lead to significant prediction errors. To address this limitation, we enhance feature extraction and expressiveness by integrating a multi-timescale feature fusion network. As shown in **Figure 2c**, the raw 1D data is transformed into 2D images of varying dimensions. These are processed through parallel submodels for independent training and optimization, with final predictions generated via weighted averaging of all submodel outputs. Critically, the weights are learnable parameters during model training.

**Training optimization**. The AdamW optimizer is employed to enhance model generalizability during parameter updates [110]. Neural network parameters are optimized by minimizing the mean squared error (MSE) loss function. Learning rates are adaptively adjusted based on validation MSE performance. Hyperparameter optimization is conducted using Bayesian algorithms [111], where the search space includes image dimensions, kernel sizes of the first convolutional layer, channel numbers of both convolutional layers, and other key parameters, with validation MSE serving as the objective function.

**Iterative multi-step prediction**. For long-time forecasting tasks, a sliding window algorithm is applied: First, input the 2D image generated from the end of the training set into the trained model to obtain the predicted time point $\tilde{y}_1$. Next, remove the initial time point from the original image, append $\tilde{y}_1$ as a new data to the image's trailing edge, and form the input features for the next time point. This process is iteratively repeated until the desired prediction sequence length is achieved. Model performance is evaluated using the mean absolute error (MAE):

$$\mathrm{MAE} = \frac{1}{n}\sum_{i=1}^{n}|y_i - \tilde{y}_i|, \tag{1}$$

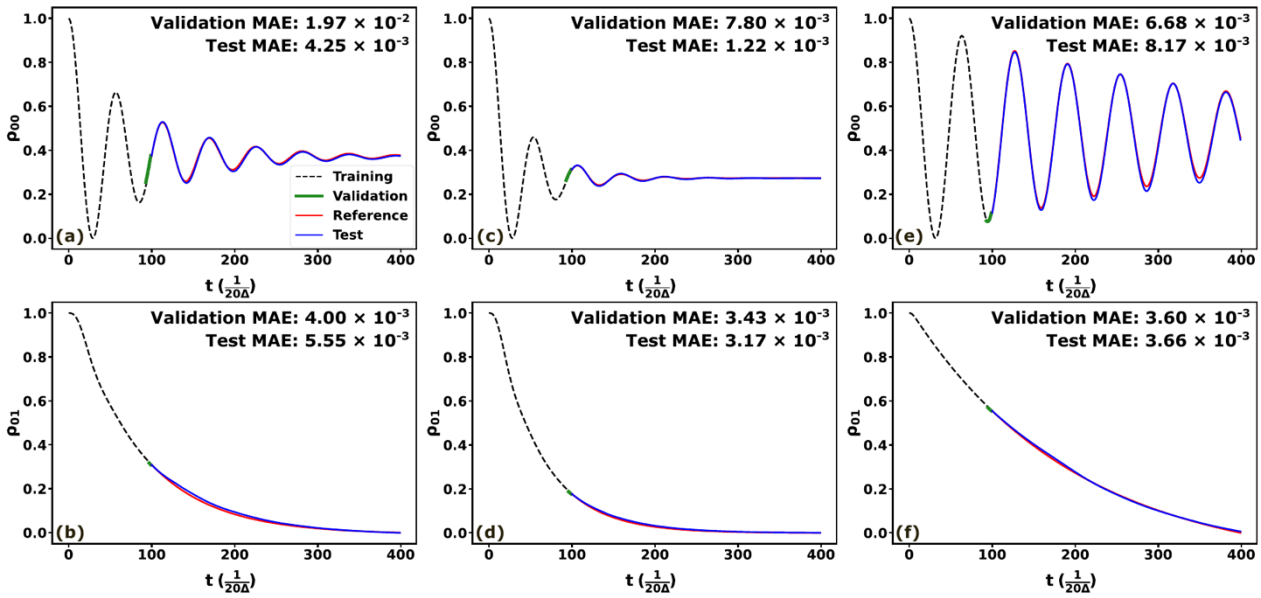


**Figure 3.** Time evolution of RDM elements $\rho_{00}$ and $\rho_{01}$ for three spin-boson models using 2D-CNN networks. (a) and (b) correspond to $\rho_{00}$ and $\rho_{01}$ of the system with $\gamma = 1.0$, $\beta = 0.5$. (c) and (d) correspond to $\rho_{00}$ and $\rho_{01}$ of the system with $\gamma = 1.0$, $\beta = 0.25$. (e) and (f) correspond to $\rho_{00}$ and $\rho_{01}$ of the system with $\gamma = 1.0$, $\beta = 0.25$. All parameters are in units of Δ. Validation and test MAEs are provided in each subplot.

where $y_i$ denote reference values computed via HEOM, $\tilde{y}_i$ represents the model-predicted values, and $n$ is the total number of samples (i.e., time points).

The 2D-CNN models were implemented using the PyTorch framework [112], with computations accelerated via an NVIDIA GeForce RTX 4090 24GB graphics processing unit (GPU). All reference data were generated by HEOM-QUICK2 [113], a program for general-purpose simulations of open quantum systems. The predictive performance of the proposed 2D-CNN models is exemplified by two numerical examples: (1) dissipative relaxation in a two-level system, exhibiting relatively simple dynamics characterized by low-frequency oscillatory decay; (2) Rabi oscillations in local spins coupled to environmental spins via Kondo exchange, featuring complex dynamics that include both low-frequency oscillatory decay and high-frequency Larmor precession.

## 3. Results and discussion

### 3.1 Dissipative relaxation in a two-level system

The spin-boson model describes the interaction of a two-level quantum system (such as an atom, molecule, or qubit) with a thermal bath of harmonic oscillators through linear coupling, serving as a theoretical benchmark for studying decoherence, energy relaxation, and non-adiabatic dynamics (e.g., electron transfer) in quantum dissipative systems [93, 114-117]. The Hamiltonian of the system-plus-bath composite is given by [4]:

$$\hat{H}_{\mathrm{T}} = \hat{H}_{\mathrm{S}} + \hat{H}_{\mathrm{B}} + \hat{H}_{\mathrm{SB}}, \tag{2}$$

where $\hat{H}_{\mathrm{S}} = \frac{\epsilon}{2}\hat{\sigma}_z + \frac{\Delta}{2}\hat{\sigma}_x$ , $\hat{H}_{\mathrm{B}} = \sum_k \omega_k \hat{a}_k^\dagger \hat{a}_k$ and $\hat{H}_{\mathrm{SB}} = \hat{\sigma}_z \sum_k g_k\left(\hat{a}_k^\dagger + \hat{a}_k\right)$. Here, $\epsilon$ is the energy gap between the two system levels ($|0\rangle$ and $|1\rangle$). Δ is the tunneling matrix element. $\hat{\sigma}_z = |0\rangle\langle 0| - |1\rangle\langle 1|$ and $\hat{\sigma}_x = |0\rangle\langle 1| + |1\rangle\langle 0|$ are the Pauli operators, $\hat{a}_k^\dagger(\hat{a}_k)$ represents the creation (annihilation) operator for the $k$th bath mode with frequency $\omega_k$, and $g_k$ are the system-bath coupling coefficients.

The influence of a Gaussian bath on the reduced system dynamics is fully determined by the bath spectral density function. Here, we adopt the Drude spectral density [4]:

$$J(\omega) \equiv \pi \sum_k g_k^2\, \delta(\omega_k - \omega) = \frac{2\lambda\omega\gamma}{\omega^2 + \gamma^2}, \tag{3}$$

where $\lambda$ is the bath reorganization energy, which governs the system-bath coupling strength.

The reduced system dynamics is described by the time evolution of the RDM,

$$\rho(t) = \mathrm{Tr}_{\mathrm{B}}[\rho_{\mathrm{T}}(t)] \tag{4}$$

where $\rho_{\mathrm{T}}$ is the density matrix of the total system. Initially, the composite system is assumed to be in a factorized state, $\rho_{\mathrm{T}}(0) = \rho(0)\rho_{\mathrm{B}}^{\mathrm{eq}}$, with $\rho(0) = |0\rangle\langle 0|$ and

$$\rho_{\mathrm{B}}^{\mathrm{eq}} = \frac{e^{-\beta\hat{H}_{\mathrm{B}}}}{\mathrm{Tr}_{\mathrm{B}}(e^{-\beta\hat{H}_{\mathrm{B}}})} \quad \text{where} \quad \beta = \frac{1}{k_{\mathrm{B}}T}.$$

Here, $T$ is the temperature and $k_{\mathrm{B}}$ is the Boltzmann constant.

We selected four trajectories of the RDM dynamics for the spin-boson system from the QD3SET-1 database [118], simulated using the HEOM method. These trajectories cover parameter values of $\epsilon = 0.0$, $\lambda = 0.1$, $\gamma = 1.0$ or $10.0$, $\beta = 0.1$, $0.25$, $0.5$ or $1.0$, all given in units of Δ. Each trajectory has a step size of $dt = 0.05/\Delta$ and a total length of $t_{\max} = 20/\Delta$. The training, validation, and test datasets cover intervals of $t = 4.5/\Delta$, $t = 0.5/\Delta$ and $t = 15/\Delta$, respectively. For each trajectory, we trained on either the diagonal or off-diagonal RDM elements for 1000 epochs and saved the model with the lowest validation MSE for long-time dynamics prediction.

Predicting off-diagonal element dynamics proved more challenging than diagonal elements, likely due to their dependence on longer historical dynamic ranges, while the available training data were relatively short. To address this, we implemented a multi-

timescale feature fusion network with two models: Model_2 processes a 2D image input with twice the width $W$ of that used by Model_1.

As shown in **Figure 3**, the model-predicted dynamics trajectories for both diagonal and off-diagonal elements of the RDM exhibit excellent agreement with the HEOM reference results, achieving validation and test MAEs on the order of $10^{-3}$. The test MAEs of our model are on the same order of magnitude as those of the artificial neural network-based models in prior work by Rodríguez et al. [76]. These results confirm that the 2D-CNN architecture is capable of capturing the non-Markovian memory effects inherent to the dissipative dynamics of open quantum systems.

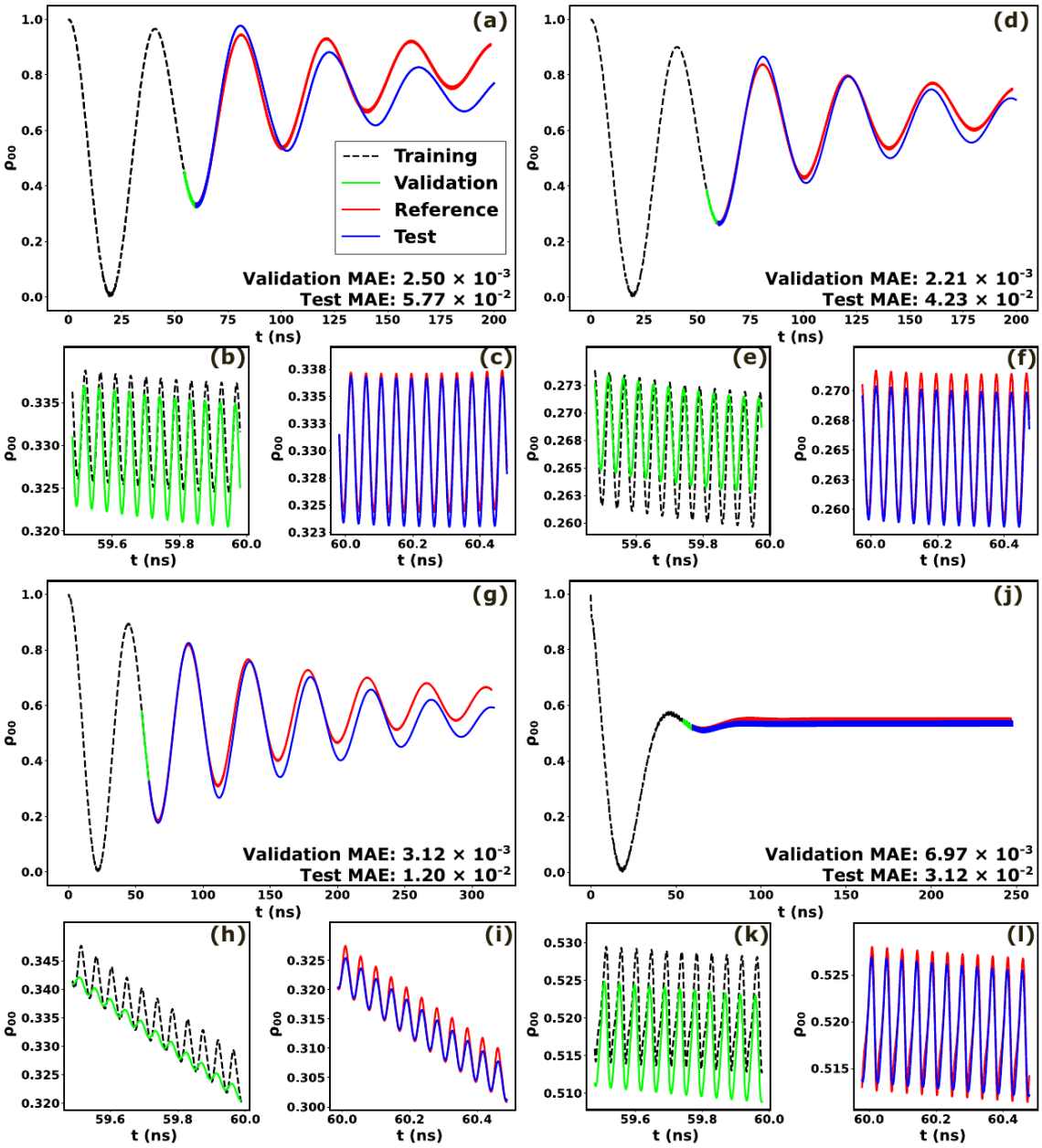


**Figure 4.** Time evolution of $\rho_{00}$ for an extended AIM predicted by the 2D-CNN model. (a) Results with $V_{\mathrm{RF}} = 0.20$ mV and different bandwidths for the two electron reservoirs. (d) Dynamics under a different initial state compared to (a), with all other parameters unchanged. (g) Results with $V_{\mathrm{RF}} = 0.20$ mV and identical bandwidths for the two electron reservoirs. (j) Results with $V_{\mathrm{RF}} = 0.25$ mV and different bandwidths for the two electron reservoirs. (b, c), (e, f), (h, i), and (k, l) show zoom-in views of panels (a), (d), (g) and (j), respectively. (b, e, h, k) display the model predictions for the final 5,000 validation data points. (c, f, i, l) display the model predictions for the first 5,000 test data points.

### 3.2 Rabi oscillation of dissipative local spins

Recent advancements in STM-RF technology [99, 100, 119-122] have enabled real-time coherent control of local spin states of surface atoms and molecules through time-varying RF voltage ($V_{\mathrm{RF}}$) pulses. Motivated by these experimental breakthroughs, several theoretical studies have emerged [123-125]. For instance, an extended Anderson impurity model (AIM) [123, 125-128] has been employed to describe Rabi oscillations of local spins coupled to environmental spins through Kondo exchange interactions. The total Hamiltonian consists of three parts: $\hat{H}_{\mathrm{AIM}} = \hat{H}_{\mathrm{imp}} + \hat{H}_{\mathrm{env}} + \hat{H}_{\mathrm{coup}}$, where

$$\hat{H}_{\mathrm{AIM}} = \sum_{\nu=1,2} \epsilon_\nu(\hat{n}_{\nu\uparrow} + \hat{n}_{\nu\downarrow}) + U_\nu \hat{n}_{\nu\uparrow}\hat{n}_{\nu\downarrow}$$

$$+g_1\mu_{\mathrm{B}}\left(\boldsymbol{B}_{ext} + \boldsymbol{B}_{\mathrm{tip}}^{\mathrm{dir}}\right)\cdot\hat{S}_1 + g_2\mu_{\mathrm{B}}\boldsymbol{B}_{\mathrm{ext}}\cdot\hat{S}_2$$

$$+J\hat{S}_1\cdot\hat{S}_2 + D\left(3\hat{S}_1^z\hat{S}_2^z - \hat{S}_1\cdot\hat{S}_2\right). \qquad (5)$$

Here, $\hat{n}_\nu = \sum_\sigma \hat{a}_{\nu\sigma}^\dagger \hat{a}_{\nu\sigma}$ is the electron number operator for the $\nu$th impurity orbital, where $\hat{a}_{\nu\sigma}^\dagger(\hat{a}_{\nu\sigma})$ is the creation (annihilation) operator for a spin-$\sigma$ ($\sigma = \uparrow, \downarrow$) electron. $\epsilon_\nu$ represents the orbital energy, and $U_\nu$ is the intra-orbital Coulomb repulsion energy. $\hat{S}_\nu$ denotes the spin operator associated with $\nu$th orbital, with $g_\nu$ being the gyromagnetic ratio and $\mu_{\mathrm{B}}$ the Bohr magneton. $J$ and $D$ represent the exchange and dipolar coupling strengths between the two local spins, respectively. $\boldsymbol{B}_{\mathrm{ext}}$ is an external static magnetic field and $\boldsymbol{B}_{\mathrm{tip}}^{\mathrm{dir}}$ is the static magnetic field generated by the permanent spin moment of Fe atoms at the apex of the STM tip. The environment consists of the surface substrate and the STM tip, which are treated as two electron reservoirs with identical or different bandwidths.

Numerical simulations have revealed that when the frequency of the $V_{\mathrm{RF}}$ matches an impurity's Zeeman splitting, electron population on the impurity orbital and its associated local spin exhibit periodic Rabi oscillations with a decaying magnitude [128], as characterized by

$$P(t) \approx P_0 e^{-t/T^{\mathrm{Rabi}}} \sin(\Omega t + \phi_0) \times [1 + A\sin(\omega_L t + \phi_1)] + P_1. \qquad (6)$$

Here, $P_0$, $P_1$, $\Omega$, $\phi_0$ and $T^{\mathrm{Rabi}}$ are the amplitude, offset, frequency, phase, and coherence time of the Rabi oscillation, respectively. $\omega_L$, $\phi_1$ and $A$ are the frequency, phase and amplitude of the Larmor precession, respectively. Although HEOM calculations nicely reproduce the experimental observations, the computations for producing the long-time quantum dissipative dynamics are rather intensive. For instance, simulating a 200 ns Rabi oscillation trajectory, containing 2,000,000 data points, requires a total CPU runtime of 2,974 s with 48 CPU cores running in parallel mode.

To overcome the limitations in computational efficiency, the aforementioned 2D-CNN model is applied to predict the long-time spin dynamics driven by $V_{\mathrm{RF}}$. We selected four representative Rabi oscillation trajectories, encompassing typical features such as high-frequency Larmor precession and low-frequency oscillation decay, with evolution durations ranging from 200 to 320 ns. When generating dynamical trajectories, different $V_{\mathrm{RF}}$ (0.20 mV or 0.25 mV), various initial states, and either identical or different bandwidths of electron reservoirs [113] were employed to verify the universality of our model. The first 60 ns of time evolution data were chosen and divided into training and validation sets at a 9: 1 ratio. A multi-timescale fusion method with three models is employed, with the input image widths $W$ for Model_1, Model_2 and Model_3 being $x$, $2x$ and $3x$, respectively.

The results are shown in **Figure 4**. The validation and test MAEs are on the order of $10^{-3}$ and $10^{-2}$, respectively. While the test MAE exceeds that of the spin-boson system, the Rabi oscillation dynamics are inherently more complex than the dissipative relaxation of a two-level system, owing to their multi-timescale features and substantially prolonged coherence times. Our 2D-CNN model demonstrates robust capability in capturing these intricate dynamics. Remarkably, the model generates predictions in a GPU runtime of 715 s, compared to the total CPU runtime of 142,758 s required by the HEOM method. Moreover, it is important to emphasize that, HEOM computational costs grow exponentially with system size, whereas those of the 2D-CNN model scale linearly.

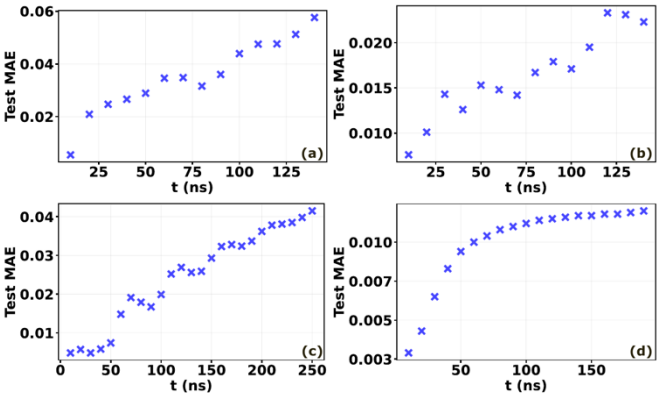


**Figure 5.** Variation of test MAE with respect to the final time $t$ under prediction for various dynamics trajectories. Panels (a), (b), (c) and (d) correspond to the trajectories from **Figure 4(a), (d), (g)** and **(j)**, respectively.

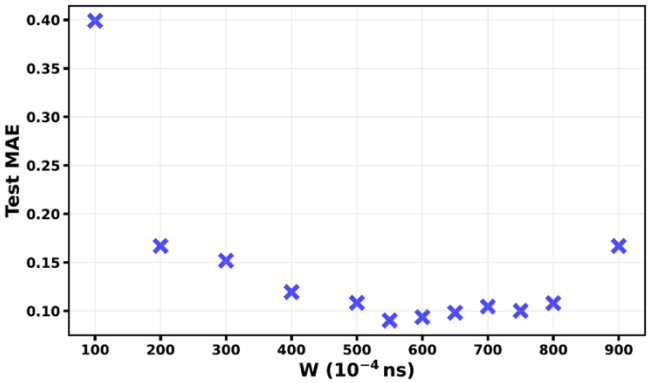


**Figure 6.** Parameter sensitivity analysis with the size of sliding window $W$ as the key parameter, using the trajectory from **Figure 4(a)** as an example.

It is worth pointing out that the test MAE defined by **Equation (1)** may vary with the final time $t$ for prediction, particularly when the system under study is far away from a steady state. To explicitly illustrate this phenomenon, we analyzed the relationship between test MAE and $t$ for each system in **Figure 4**, with the results shown in **Figure 5**. In **Figure 5(d)**, test MAE exhibits a convergent trend as $t$ increases, i.e., test MAE tends to approach a constant with increasing $t$, whereas no such convergence is observed in **Figure 5(a-c)**. This discrepancy possibly results from the dynamic evolution having reached a steady state in **(d)**, while the systems in **(a-c)** have not yet reached such a state.

Furthermore, a parameter sensitivity analysis was carried out to validate the robustness of our model. The size of sliding window $W$ was employed as the key parameter due to its length directly influencing the richness of dynamical information. The result is shown in **Figure 6**. When $W$ varies within a wide range from 0.05 to 0.08 ns, test MAE changes only slightly, indicating that our model exhibits strong robustness. This result also implies that when an optimized model is obtained, its hyperparameters require only minor

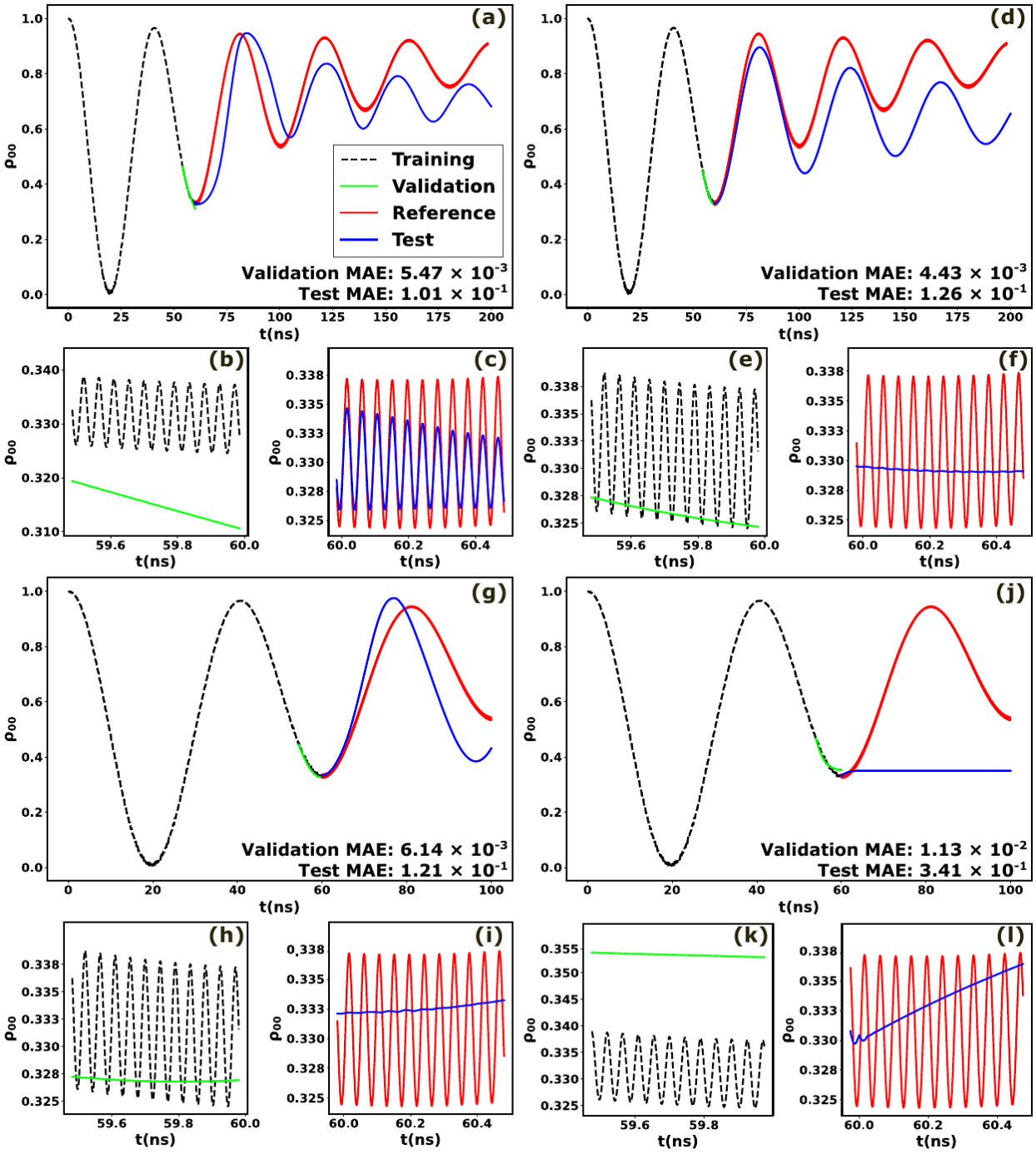


**Figure 7.** Time evolution of $\rho_{00}$ for an extended AIM predicted by various models. The trajectory from **Figure 4(a)** is using as an example. (a) Dynamics predicted by 1D-CNN model. (d) Dynamics predicted by single model without multi-timescale feature fusion network. (g) Dynamics predicted by 2D-CNN-LSTM model. (j) Dynamics predicted by LSTM model. (b, c), (e, f), (h, i), and (k, l) show zoom-in views of panels (a), (d), (g) and (j), respectively. (b, e, h, k) display the model predictions for the final 5,000 validation data points. (c, f, i, l) display the model predictions for the first 5,000 test data points.

adjustments to be applied to new dynamic trajectories, thereby significantly reducing the cost of hyperparameter optimization.

To evaluate the performance improvement enabled by the "1D-to-2D" feature reconstruction strategy and the multi-timescale feature fusion techniques, we retrained the model using the trajectory from **Figure 4(a)**. The results reveal that validation and test MAEs increase to $10^{-3}$ and $10^{-1}$, respectively, when the 1D-CNN model is employed; see **Figure 7(a-c)**. This improvement arises because 2D images, unlike 1D sequential data, better capture multi-timescale features. Specifically, high- and low-frequency oscillations and temporal decay are encoded along the horizontal and vertical dimensions of the 2D matrix. When only a single model is used, validation and test MAEs also rise to $10^{-3}$ and $10^{-1}$, respectively, as shown in **Figure 7(d-f)**. This result confirms the technique's effectiveness, which may contribute to higher model complexity and stronger multi-timescale representation capability of the feature fusion network. Furthermore, we compared our model to 2D-CNN-LSTM model and LSTM model using the trajectory from **Figure 4(a)**

as an example. To save the computational cost of LSTM, the length of the trajectory is truncated at 100 ns. Both 2D-CNN-LSTM and LSTM models exhibit significantly higher validation and test MAEs compared to our proposed model, as presented in **Figure 7(g-l)**. Additionally, they require much more computational resources, with GPU runtime of 4,913 s and 13,196 s, respectively, compared to just 143 s of our model. These comparative results highlight the remarkable advantages of our 2D-CNN model in achieving superior accuracy and computational efficiency when handling long-time quantum dissipative dynamics with multi-timescale features.

## 4. Conclusion

To summarize, we have developed a deep learning framework based on a 2D-CNN to efficiently predict the long-time evolution of quantum dissipative systems using only short-time historical dynamics data. By reconstructing 1D time-series data into interpretable 2D images, the framework successfully resolves dynamical patterns across multiple timescales. This approach achieves low test MAEs in simulating both dissipative relaxation in a two-level system and Rabi oscillations in a dissipative spin system, demonstrating its versatility in modeling complex open quantum systems. Compared to traditional numerically rigorous methods such as HEOM, our framework reduces computational costs by orders of magnitude while maintaining accuracy, offering a practical tool for large-scale, long-time quantum dynamics simulations.

A current limitation is the need for hyperparameter re-optimization when applied to systems with differing initial states. Future research will focus on enhancing the model's representational capacity, generalization across diverse initial conditions, and robustness in extreme parameter regimes.

## Acknowledgements

The support from the National Natural Science Foundation of China (Grants No. 22393912 and No. 22425301), the AI for Science Foundation of Fudan University (Grant No. FudanX24AI023), Innovation Program for Quantum Science and Technology (Grant No. 2021ZD0303306), and Strategic Priority Research Program of the Chinese Academy of Sciences (Grant No. XDB0450101) is gratefully acknowledged.

## References

[1] Nielsen M.A., Chuang I.L., Quantum Computation and Quantum Information: 10th Anniversary Edition., Cambridge University Press, Cambridge, 2010.

[2] Xu D., Schulten K., Coupling of protein motion to electron transfer in a photosynthetic reaction center: investigating the low temperature behavior in the framework of the spin—boson model. *Chem. Phys.*, **182** (1994), 91-117.

[3] Ishizaki A., Fleming G.R., Quantum coherence in photosynthetic light harvesting. *Annu. Rev. Condens. Matter Phys.*, **3** (2012), 333-361.

[4] Weiss U., Quantum Dissipative Systems., 4th ed., WORLD SCIENTIFIC, Singapore, 2012.

[5] Breuer H.-P., Petruccione F., The Theory of Open Quantum Systems., Oxford University Press, Oxford, 2007.

[6] Leggett A.J., Chakravarty S., Dorsey A.T., Fisher M.P.A., Garg A., Zwerger W., Dynamics of the dissipative two-state system. *Rev. Mod. Phys.*, **59** (1987), 1-85.

[7] May V., Kühn O., Excitation Energy Transfer., John Wiley and Sons Ltd, Hoboken, 2011.

[8] Wilson K.G., The renormalization group: critical phenomena and the kondo problem. *Rev. Mod. Phys.*, **47** (1975), 773-840.

[9] Bulla R., Costi T.A., Pruschke T., Numerical renormalization group method for quantum impurity systems. *Rev. Mod. Phys.*, **80** (2008), 395-450.

[10] Pižorn I., Verstraete F., Variational numerical renormalization group: bridging the gap between NRG and density matrix renormalization group. *Phys. Rev. Lett.*, **108** (2012), 067202.

[11] Schwarz F., Weymann I., von Delft J., Weichselbaum A., Nonequilibrium steady-state transport in quantum impurity models: a thermofield and quantum quench approach using matrix product states. *Phys. Rev. Lett.*, **121** (2018), 137702.

[12] Kugler F.B., Improved estimator for numerical renormalization group calculations of the self-energy. *Phys. Rev. B*, **105** (2022), 245132.

[13] Anders F.B., Schiller A., Real-time dynamics in quantum-impurity systems: a time-dependent numerical renormalization-group approach. *Phys. Rev. Lett.*, **95** (2005), 196801.

[14] Eidelstein E., Schiller A., Güttge F., Anders F.B., Time-dependent numerical renormalization group approach to nonequilibrium quantum impurity systems. *Phys. Rev. B*, **85** (2012), 075118.

[15] Nghiem H.T.M., Costi T.A., Generalization of the time-dependent numerical renormalization group method to finite temperatures and general pulses. *Phys. Rev. B*, **89** (2014), 075118.

[16] Nghiem H.T.M., Costi T.A., Time-dependent numerical renormalization group method for multiple quenches: towards exact results for the long-time limit of thermodynamic observables and spectral functions. *Phys. Rev. B*, **98** (2018), 155107.

[17] Nghiem H.T.M., Costi T.A., Self-energy method for time-dependent spectral functions of the Anderson impurity model within the time-dependent numerical renormalization group approach. *Phys. Rev. B*, **104** (2021), 205113.

[18] Blankenbecler R., Scalapino D.J., Sugar R.L., Monte Carlo calculations of coupled boson-fermion systems. I. *Phys. Rev. D*, **24** (1981), 2278-2286.

[19] Ceperley D., Alder B., Quantum Monte Carlo. *Science*, **231** (1986), 555-560.

[20] Foulkes W.M.C., Mitas L., Needs R.J., Rajagopal G., Quantum Monte Carlo simulations of solids. *Rev. Mod. Phys.*, **73** (2001), 33-83.

[21] Van Houcke K., Kozik E., Prokof'ev N., Svistunov B., Diagrammatic Monte Carlo. *Phys. Procedia*, **6** (2010), 95-105.

[22] Schiró M., Real-time dynamics in quantum impurity models with diagrammatic Monte Carlo. *Phys. Rev. B*, **81** (2010), 085126.

[23] Sandvik A.W., Computational studies of quantum spin systems. *AIP Conf. Proc.*, **1297** (2010), 135-338.

[24] Gull E., Millis A.J., Lichtenstein A.I., Rubtsov A.N., Troyer M., Werner P., Continuous-time Monte Carlo methods for quantum impurity models. *Rev. Mod. Phys.*, **83** (2011), 349-404.

[25] Carlson J., Gandolfi S., Pederiva F., Pieper S.C., Schiavilla R., Schmidt K.E., Wiringa R.B., Quantum Monte Carlo methods for nuclear physics. *Rev. Mod. Phys.*, **87** (2015), 1067-1118.

[26] Cohen G., Gull E., Reichman D.R., Millis A.J., Taming the dynamical sign problem in real-time evolution of quantum many-body problems. *Phys. Rev. Lett.*, **115** (2015), 266802.
[27] Antipov A.E., Dong Q., Kleinhenz J., Cohen G., Gull E., Currents and Green's functions of impurities out of equilibrium: results from inchworm quantum Monte Carlo. *Phys. Rev. B*, **95** (2017), 085144.
[28] Maček M., Dumitrescu P.T., Bertrand C., Triggs B., Parcollet O., Waintal X., Quantum quasi-Monte Carlo technique for many-body perturbative expansions. *Phys. Rev. Lett.*, **125** (2020), 047702.
[29] Li J., Yu Y., Gull E., Cohen G., Interaction-expansion inchworm Monte Carlo solver for lattice and impurity models. *Phys. Rev. B*, **105** (2022), 165133.
[30] Erpenbeck A., Gull E., Cohen G., Quantum Monte Carlo method in the steady state. *Phys. Rev. Lett.*, **130** (2023), 186301.
[31] Makarov D.E., Makri N., Path integrals for dissipative systems by tensor multiplication: condensed-phase quantum dynamics for arbitrarily long time. *Chem. Phys. Lett.*, **221** (1994), 482-491.
[32] Mühlbacher L., Rabani E., Real-time path integral approach to nonequilibrium many-body quantum systems. *Phys. Rev. Lett.*, **100** (2008), 176403.
[33] Vagov A., Croitoru M.D., Glässl M., Axt V.M., Kuhn T., Real-time path integrals for quantum dots: quantum dissipative dynamics with superohmic environment coupling. *Phys. Rev. B*, **83** (2011), 094303.
[34] Strathearn A., Lovett B.W., Kirton P., Efficient real-time path integrals for non-Markovian spin-boson models. *New J. Phys.*, **19** (2017), 093009.
[35] Bose A., Makri N., All-mode quantum–classical path integral simulation of bacteriochlorophyll dimer exciton-vibration dynamics. *J. Phys. Chem. B*, **124** (2020), 5028-5038.
[36] Ye E., Chan G.K.-L., Constructing tensor network influence functionals for general quantum dynamics. *J. Chem. Phys.*, **155** (2021), 044104.
[37] Thoenniss J., Lerose A., Abanin D.A., Nonequilibrium quantum impurity problems via matrix-product states in the temporal domain. *Phys. Rev. B*, **107** (2023), 195101.
[38] Tanimura Y., Kubo R., Time evolution of a quantum system in contact with a nearly Gaussian-Markoffian noise bath. *J. Phys. Soc. Jpn.*, **58** (1989), 101-114.
[39] Tanimura Y., Kubo R., Two-time correlation functions of a system coupled to a heat bath with a Gaussian-Markoffian interaction. *J. Phys. Soc. Jpn.*, **58** (1989), 1199-1206.
[40] Tanimura Y., Nonperturbative expansion method for a quantum system coupled to a harmonic-oscillator bath. *Phys. Rev. A*, **41** (1990), 6676-6687.
[41] Yan Y., Yang F., Liu Y., Shao J., Hierarchical approach based on stochastic decoupling to dissipative systems. *Chem. Phys. Lett.*, **395** (2004), 216-221.
[42] Xu R.-X., Cui P., Li X.-Q., Mo Y., Yan Y., Exact quantum master equation via the calculus on path integrals. *J. Chem. Phys.*, **122** (2005), 041103.
[43] Tanimura Y., Stochastic Liouville, Langevin, Fokker-Planck, and master equation approaches to quantum dissipative systems. *J. Phys. Soc. Jpn.*, **75** (2006), 082001.
[44] Xu R.-X., Yan Y., Dynamics of quantum dissipation systems interacting with bosonic canonical bath: hierarchical equations of motion approach. *Phys. Rev. E*, **75** (2007), 031107.
[45] Tanimura Y., Numerically "exact" approach to open quantum dynamics: the hierarchical equations of motion (HEOM). *J. Chem. Phys.*, **153** (2020), 020901.
[46] Ding X., Zhang D., Ye L., Zheng X., Yan Y., On the practical truncation tier of fermionic hierarchical equations of motion. *J. Chem. Phys.*, **157** (2022), 224107.
[47] Meyer H.-D., Manthe U., Cederbaum L., The multi-configurational time-dependent Hartree approach. *Chem. Phys. Lett.*, **165** (1990), 73-78.
[48] Beck M., Jäckle A., Worth G., Meyer H.-D., The multiconfiguration time-dependent Hartree (MCTDH) method: a highly efficient algorithm for propagating wavepackets. *Phys. Rep.*, **324** (2000), 1-105.
[49] Wang H., Thoss M., Multilayer formulation of the multiconfiguration time-dependent Hartree theory. *J. Chem. Phys.*, **119** (2003), 1289-1299.
[50] Manthe U., A multilayer multiconfigurational time-dependent Hartree approach for quantum dynamics on general potential energy surfaces. *J. Chem. Phys.*, **128** (2008), 164116.
[51] Zheng J., Xie Y., Jiang S., Lan Z., Ultrafast nonadiabatic dynamics of singlet fission: quantum dynamics with the multilayer multiconfigurational time-dependent Hartree (ML-MCTDH) method. *J. Phys. Chem. C*, **120** (2016), 1375-1389.
[52] Wang H., Meyer H.-D., On regularizing the ML-MCTDH equations of motion. *J. Chem. Phys.*, **149** (2018), 044119.
[53] Wang H., Thoss M., A multilayer multiconfigurational time-dependent Hartree study of the nonequilibrium Anderson impurity model at zero temperature. *Chem. Phys.*, **509** (2018), 13-19.
[54] Wang H., Thoss M., Numerically exact quantum dynamics for indistinguishable particles: the multilayer multiconfiguration time-dependent Hartree theory in second quantization representation. *J. Chem. Phys.*, **131** (2009), 024114.
[55] Cazalilla M.A., Marston J.B., Time-dependent density-matrix renormalization group: a systematic method for the study of quantum many-body out-of-equilibrium systems. *Phys. Rev. Lett.*, **88** (2002), 256403.
[56] Schollwöck U., The density-matrix renormalization group. *Rev. Mod. Phys.*, **77** (2005), 259-316.
[57] Güttge F., Anders F.B., Schollwöck U., Eidelstein E., Schiller A., Hybrid NRG-DMRG approach to real-time dynamics of quantum impurity systems. *Phys. Rev. B*, **87** (2013), 115115.
[58] Schuch N., Bauer B., Matrix product state algorithms for Gaussian fermionic states. *Phys. Rev. B*, **100** (2019), 245121.
[59] Jansen D., Bonča J., Heidrich-Meisner F., Finite-temperature density-matrix renormalization group method for electron-phonon systems: thermodynamics and Holstein-polaron spectral functions. *Phys. Rev. B*, **102** (2020), 165155.
[60] Barcza G., Bauerbach K., Eickhoff F., Anders F.B., Gebhard F., Legeza O., Symmetric single-impurity Kondo model on a tight-binding chain: comparison of analytical and numerical ground-state approaches. *Phys. Rev. B*, **101** (2020), 075132.
[61] White S.R., Feiguin A.E., Real-time evolution using the density matrix renormalization group. *Phys. Rev. Lett.*, **93** (2004), 076401.
[62] Büsser C.A., Heidrich-Meisner F., Inducing spin correlations and entanglement in a double quantum dot through

nonequilibrium transport. *Phys. Rev. Lett.*, **111** (2013), 246807.65 – 128

[63] Ren J., Shuai Z., Chan G. K-L., Time-dependent density matrix renormalization group algorithms for nearly exact absorption and fluorescence spectra of molecular aggregates at both zero and finite temperature. *J. Chem. Theory Comput.*, **14** (2018), 5027-5039.

[64] Xie X., Liu Y., Yao Y., Schollwöck U., Liu C., Ma H., Time-dependent density matrix renormalization group quantum dynamics for realistic chemical systems. *J. Chem. Phys.*, **151** (2019), 224101.

[65] Baiardi A., Electron dynamics with the time-dependent density matrix renormalization group. *J. Chem. Theory Comput.*, **17** (2021), 3320-3334.

[66] Diósi L., Strunz W.T., The non-Markovian stochastic Schrödinger equation for open systems. *Phys. Lett. A*, **235** (1997), 569-573.

[67] Bouten L., Guta M., Maassen H., Stochastic Schrödinger equations. *J. Phys. A: Math. Gen.*, **37** (2004), 3189-3189.

[68] Han L., Chemyak V., Yan Y.-A., Zheng X., Yan Y., Stochastic representation of non-Markovian fermionic quantum dissipation. *Phys. Rev. Lett.*, **123** (2019), 050601.

[69] Gao X., Ren J., Eisfeld A., Shuai Z., Non-Markovian stochastic Schrödinger equation: matrix-product-state approach to the hierarchy of pure states. *Phys. Rev. A*, **105** (2022), L030202.

[70] Luo S., Lambert N., Liang P., Crio M., Quantum-classical decomposition of Gaussian quantum environments: a stochastic pseudomode model. *PRX Quantum*, **4** (2023), 030316.

[71] Yan Y.-A., Shao J., Exact dynamics of the spin-boson model at the Toulouse limit. *Phys. Rev. A*, **108** (2023), 012218.

[72] Stefanucci G., Kurth S., Steady-state density functional theory for finite bias conductances. *Nano Lett.*, **15** (2015), 8020-8025.

[73] Cerrillo J., Cao J., Non-Markovian dynamical maps: numerical processing of open quantum trajectories. *Phys. Rev. Lett.*, **112** (2014), 110401.

[74] Kananenka A.A., Hsieh C.-Y., Cao J., Geva E., Accurate long-time mixed quantum-classical Liouville dynamics via the transfer tensor method. *J. Phys. Chem. Lett.*, **7** (2016), 4809-4814.

[75] Gelzinis A., Rybakova E., Valkunas L., Applicability of transfer tensor method for open quantum system dynamics. *J. Chem. Phys.*, **147** (2017), 234108.

[76] Rodríguez L.E.H., Ullah A., Espinosa K.J.R., Dral P.O., Kananenka A.A., A comparative study of different machine learning methods for dissipative quantum dynamics. *Mach. Learn.: Sci. Technol.*, **3** (2022), 045016.

[77] LeCun Y., Bengio Y., Hinton G., Deep learning. *Nature*, **521** (2015), 436-444.

[78] Häse F., Kreisbeck C., Aspuru-Guzik A., Machine learning for quantum dynamics: deep learning of excitation energy transfer properties. *Chem. Sci.*, **8** (2017), 8419-8426.

[79] Bandyopadhyay S., Huang Z., Sun K., Zhao Y., Applications of neural networks to the simulation of dynamics of open quantum systems. *Chem. Phys.*, **515** (2018), 272-278.

[80] Hartmann M.J., Carleo G., Neural-network approach to dissipative quantum many-body dynamics. *Phys. Rev. Lett.*, **122** (2019), 250502.

[81] Yang B., He B., Wan J., Kubal S., Zhao Y., Applications of neural networks to dynamics simulation of Landau-Zener transitions. *Chem. Phys.*, **528** (2020), 110509.

[82] Ullah A., Dral P.O., Speeding up quantum dissipative dynamics of open systems with kernel methods. *New J. Phys.*, **23** (2021), 113019.

[83] Secor M., Soudackov A.V., Hammes-Schiffer S., Artificial neural networks as propagators in quantum dynamics. *J. Phys. Chem. Lett.*, **12** (2021), 10654-10662.

[84] Akimov A.V., Extending the time scales of nonadiabatic molecular dynamics via machine learning in the time domain. *J. Phys. Chem. Lett.*, **12** (2021), 12119-12128.

[85] Banchi L., Grant E., Rocchetto A., Severini S., Modelling non-Markovian quantum processes with recurrent neural networks. *New J. Phys.*, **20** (2018), 123030.

[86] Lin K., Peng J., Gu F.L., Lan Z., Simulation of open quantum dynamics with bootstrap-based long short-term memory recurrent neural network. *J. Phys. Chem. Lett.*, **12** (2021), 10225-10234.

[87] Lin K., Peng J., Xu C., Gu F.L., Lan Z., Automatic evolution of machine-learning-based quantum dynamics with uncertainty analysis. *J. Chem. Theory Comput.*, **18** (2022), 5837-5855.

[88] Lin K., Peng J., Xu C., Gu F.L., Lan Z., Machine-learning-based quantum dynamics: predicting nonadiabatic processes. *arXiv preprint*, (2022), DOI: 10.48550/arXiv:2207.05556.

[89] Herrera Rodríguez L.E., Kananenka A.A., Convolutional neural networks for long-time dissipative quantum dynamics. *J. Phys. Chem. Lett.*, **12** (2021), 2476-2483.

[90] Ullah A., Dral P.O., Predicting the future of excitation energy transfer in light-harvesting complex with artificial intelligence-based quantum dynamics. *Nat. Commun.*, **13** (2022), 1930.

[91] Ullah A., Dral P.O., One-shot trajectory learning of open quantum systems dynamics. *J. Phys. Chem. Lett.*, **13** (2022), 6037-6041.

[92] Wu D., Hu Z., Li J., Sun X., Forecasting nonadiabatic dynamics using hybrid convolutional neural network/long short-term memory network. *J. Chem. Phys.*, **155** (2021), 224104.

[93] Leggett A.J., Chakravarty S., Dorsey A.T., Fisher M.P.A., Garg A., Zwerger W., Dynamics of the dissipative two-state system. *Rev. Mod. Phys.*, **59** (1987), 1-85.

[94] Adolphs J., Renger T., How proteins trigger excitation energy transfer in the FMO complex of green sulfur bacteria. *Biophys. J.*, **91** (2006), 2778-2794.

[95] Ishizaki A., Fleming G.R., Theoretical examination of quantum coherence in a photosynthetic system at physiological temperature. *Proc. Natl. Acad. Sci.*, **106** (2009), 17255-17260.

[96] Panitchayangkoon G., Hayes D., Fransted K.A., Caram J.R., Harel E., Wen J., Blankenship R.E., Engel G.S., Long-lived quantum coherence in photosynthetic complexes at physiological temperature. *Proc. Natl. Acad. Sci.*, **107** (2010), 12766-12770.

[97] Karafyllidis I.G., Quantum transport in the FMO photosynthetic light-harvesting complex. *J. Biol. Phys.*, **43** (2017), 239-245.

[98] Zeng H., Kou Y., Sun X., How sophisticated are neural networks needed to predict long-term nonadiabatic dynamics? *J. Chem. Theory Comput.*, **20** (2024), 9832-9848.

[99] Yang K., Paul W., Phark S.-H., Willke P., Bae Y., Choi T., Esat T., Ardavan A., Heinrich A.J., Lutz C.P., Coherent spin manipulation of individual atoms on a surface. *Science*, **366** (2019), 509-512.

[100] Willke P., Bilgeri T., Zhang X., Wang Y., Wolf C., Aubin H., Heinrich A., Choi T., Coherent spin control of single molecules on a surface. *ACS Nano*, **15** (2021), 17959-17965.

[101] Natterer F.D., Yang K., Paul W., Willke P., Choi T., Greber T., Heinrich A.J., Lutz C.P., Reading and writing single-atom magnets. *Nature*, **543** (2017), 226-228.

[102] Wang Y., Chen Y., Bui H.T., Wolf C., Haze M., Mier C., Kim J., Choi D.-J., Lutz C.P., Bae Y., Phark S., Heinrich A.J., An atomic-scale multi-qubit platform. *Science*, **382** (2023), 87-92.

[103] Tang G., Müller M., Rios A., Sennrich R., Unsupervised neural machine translation: a phrase-based approach. *arXiv preprint*, (2018), DOI: 10.48550/arXiv:1808.08946.

[104] Vaswani A., Shazeer N., Parmar N., Uszkoreit J., Jones L., Gomez A.N., Kaiser L., Polosukhin I., Attention is all you need. *arXiv preprint*, (2017), DOI: 10.48550/arXiv:1706.03762.

[105] Gehring J., Auli M., Grangier D., Yarats D., Dauphin Y.N., Convolutional sequence to sequence learning. *arXiv preprint*, (2017), DOI: 10.48550/arXiv:1705.03122.

[106] Wu H., Hu T., Liu Y., Zhou H., Wang J., Long M., Rethinking pre-training on images and text. *arXiv preprint*, (2023), DOI: 10.48550/arXiv:2210.02186.

[107] He K., Zhang X., Ren S., Sun J., Deep residual learning for image recognition. *arXiv preprint*, (2015), DOI: 10.48550/arXiv:1512.03385.

[108] Sarma A., Singh S., Jiang H., Zhang R., Kandemir M.T., Das C.R., Sensing the air pollution: a deep learning approach. *arXiv preprint*, (2021), DOI: 10.48550/arXiv:2106.12089.

[109] Zhao S.-C., Huang Y.-M., Zhao Z.-R., Predicting quantum evolutions of excitation energy transfer in a light-harvesting complex using multi-optimized recurrent neural networks. *Eur. Phys. J. Plus*, **139** (2024), 1119.

[110] Loshchilov I., Hutter F., Decoupled weight decay regularization. *arXiv preprint*, (2019), DOI: 10.48550/arXiv:1711.05101.

[111] Akiba T., Sano S., Yanase T., Ohta T., Koyama M., Optuna: a next-generation hyperparameter optimization framework. *arXiv preprint*, (2019), DOI: 10.48550/arXiv:1907.10902.

[112] Paszke A., Gross S., Massa F., Lerer A., Bradbury J., Chanan G., Killeen T., Lin Z., Gimelshein N., Antiga L., Desmaison A., Köpf A., Yang E., DeVito Z., Raison M., Tejani A., Chilamkurthy S., Steiner B., Fang L., Bai J., Chintala S., PyTorch: an imperative style, high-performance deep learning library. *arXiv preprint*, (2019), DOI: 10.48550/arXiv:1912.01703.

[113] Zhang D., Ye L., Cao J., Wang Y., Xu R.-X., Zheng X., Yan Y., HEOM-QUICK2: a general-purpose simulator for fermionic many-body open quantum systems—an update. *WIREs Comput. Mol. Sci.*, **14** (2024), e1727.

[114] Garg A., Onuchic J.N., Ambegaokar V., Effect of friction on electron transfer in biomolecules. *J. Chem. Phys.*, **83** (1985), 4491-4503.

[115] Winter A., Rieger H., Vojta M., Bulla R., Quantum phase transition in the sub-Ohmic spin-boson model: quantum Monte Carlo study with a continuous imaginary-time cluster algorithm. *Phys. Rev. Lett.*, **102** (2009), 030601.

[116] Makhlin Y., Schön G., Shnirman A., Quantum-state engineering with Josephson-junction devices. *Rev. Mod. Phys.*, **73** (2001), 357-400.

[117] Alvermann A., Fehske H., Sparse polynomial space approach to dissipative quantum systems: application to the sub-Ohmic spin-boson model. *Phys. Rev. Lett.*, **102** (2009), 150601.

[118] Ullah A., Herrera Rodríguez L.E., Dral P.O., Kananenka A.A., QD3SET-1: a database with quantum dissipative dynamics datasets. *Front. Phys.*, **11** (2023), 120235.

[119] Choi T., Paul W., Rolf-Pissarczyk S., Macdonald A.J., Natterer F.D., Yang K., Willke P., Lutz C.P., Heinrich A.J., Atomic-scale sensing of the magnetic dipolar field from single atoms. *Nat. Nanotechnol.*, **12** (2017), 420-424.

[120] Baumann S., Paul W., Choi T., Lutz C.P., Ardavan A., Heinrich A.J., Electron paramagnetic resonance of individual atoms on a surface. *Science*, **350** (2015), 417-420.

[121] Veldman L.M., Farinacci L., Rejali R., Broekhoven R., Gobeil J., Coffey D., Ternes M., Otte A.F., Free coherent evolution of a coupled atomic spin system initialized by electron scattering. *Science*, **372** (2021), 964-968.

[122] Zhang X., Wolf C., Wang Y., Aubin H., Bilgeri T., Willke P., Heinrich A.J., Choi T., Electron spin resonance of single iron phthalocyanine molecules and role of their non-localized spins in magnetic interactions. *Nat. Chem.*, **14** (2022), 59-65.

[123] Ye L., Zheng X., Xu X., Theory of electron spin resonance spectroscopy in scanning tunneling microscopy. *Phys. Rev. Lett.*, **133** (2024), 176201.

[124] Cao J., Ye L., Xu R.-X., Zheng X., The hierarchical stochastic Schrödinger equations: theory and applications. *Chin. J. Chem. Phys.*, **37** (2024), 091207.

[125] Ding X., Cao J., Zheng X., Ye L., Tracking spin flip-flop dynamics of surface molecules with quantum dissipation theory. *J. Chem. Phys.*, **162** (2025), 084114.

[126] Takemura S., Takemori N., Koga A., Valence fluctuations and electric reconstruction in the extended Anderson model on the two-dimensional Penrose lattice. *Phys. Rev. B*, **91** (2015), 165114.

[127] Craco L., Quantum orbital entanglement: a view from the extended periodic Anderson model. *Phys. Rev. B*, **77** (2008), 125122.

[128] Cao J., Long C., Ding X., Ye L., Zheng X., Unveiling coherent evolution mechanisms of molecular spin qubits by simulations of real-time spin dynamics behavior. Unpublished.